Phase flow and statistical structure of Galton-board systems

Arthur Lue* and Howard Brenner
Department of Chemical Engineering, Massachusetts Institute of Technology, Cambridge, Massachusetts 02139
(Received 2 July 1992)

Galton boards, found in museum exhibits devoted to science and technology, are often used to demonstrate visually the ubiquity of so-called "laws of probability" via an experimental realization of normal distributions. A detailed theoretical study of Galton-board phase-space dynamics and statistical behavior is presented. The study is based on a simple inelastic-collision model employing a particle falling through a spatially periodic lattice of rigid, convex scatterers. We show that such systems exhibit indeterminate behavior through the presence of strange attractors or strange repellers in phase space; nevertheless, we also show that these systems exhibit regular and predictable behavior under specific circumstances. Phase-space strange attractors, periodic attractors, and strange repellers are present in numerical simulations, confirming results anticipated from geometric analysis. The system's geometry (dictated by lattice geometry and density as well as the direction of gravity) is observed to play a dominant role in stability, phase-flow topology, and statistical observations. Smale horseshoes appear to exist in the low-lattice-density limit and may exist in other regimes. These horseshoes are generated by homoclinic orbits whose existence is dictated by system characteristics. The horseshoes lead directly to deterministic chaos in the system. Strong evidence exists for ergodicity in all attractors. Phase-space complexities are manifested at all observed levels, particularly statistical ones. Consequently, statistical observations are critically dependent upon system details. Under well-defined circumstances, these observations display behavior which does not constitute a realization of the "laws of probability."

PACS number(s): 05.45.+b, 03.20.+i, 46.10.+z

I. INTRODUCTION

Consider a Galton board consisting of inelastic pegs arranged on a vertical board in a hexagonal array. At the top, noninteracting spheres are released, colliding with the pegs as they fall under the influence of gravity. The spheres collect in bins at the bottom, and a Gaussian distribution is experimentally observed, peaked under the point of release. Moreover, the *same* Gaussian distribution is observed in replicate experiments. The Galton board is used to visually demonstrate the existence of random processes, or the so-called "laws of probability," in nature [1]; typically, an appeal is made to Bernoulli processes or binomial distributions. Ironically, the laws governing Galton-board behavior are purely deterministic; the system as a whole obeys Newton's laws of motion. We wish to establish why and under what circumstances these systems are observably random. Moreover, we wish to describe the statistical observations given known system parameters. Hence our goals go beyond the mere demonstration of Gaussian behavior. We wish to observe where such behavior fails to exist and to glean therefrom an understanding of the mechanisms that drive this and related systems.

The Galton board provides an example of a system which apparently displays complex, indeed chaotic and indeterminate, behavior while being computationally tractable and retaining physical relevance. The physical system itself resembles a crystalline medium. Our analysis may therefore underlie a rich variety of dispersive processes, leading to possible insights pertinent to novel approaches to chromatography and other separation processes [2]. As an example, we will see that there are regions where small changes in system parameters result in significant differences in system evolution characteristics, e.g., terminal velocity and diffusivity. If one wishes to separate a mixture of two types of spheres, say with close but not identical diameters or elasticities, he can find or construct a lattice such that the interaction of one type of sphere is drastically different from that of the other type of sphere. A dynamical separation process is therefore possible.

As another example, one may look to Josephson junctions. The evolution equations for the Galton board at high densities resemble those for a simple type of coupled, driven oscillator, an example of which is a special system of Josephson junctions [2]. Qualities that exist in Galton-board phase-space behavior may have analogs in the oscillator system. We will not explicitly treat these possible applications in this paper. We offer them only as possible motivations for studying this system.

How randomness originates in Galton boards is not immediately obvious. Accordingly, we will investigate the contributions of lattice geometry and density, interaction elasticity, and system symmetries to apparent randomness. We will determine the long-term behavior of Galton boards as characterized by attractors in phase space. These attractors define the qualitative nature of the system, particularly the fundamental question of whether determinate or indeterminate behavior dominates in long-time limits. We will also investigate bifurcations of the attractor under parametric changes. This will also contribute to understanding the origin of indeterminism in circumstances where it is observed to exist.

How system characteristics affect statistical observations is also not transparent. The Gaussian behavior observed in practice suggests that Galton boards manifest relatively simple diffusive attributes, at least for the classes of experiments performed. Whether this behavior is maintained under all conditions is not clear. Therefore, we will investigate the effects of parameter manipulation on ensemble average velocity and dispersion. We will investigate the existence of a mean terminal velocity and its dependence on system parameters. Moreover, we will simultaneously address the existence of diffusive behavior and deviations therefrom.

To confront these matters, the definition of "Galton board" needs to be modified. In what follows, a *Galton board* is defined as a spatially periodic array of rigid, convex scatterers possessing several key characteristics. An example is shown in Fig. 1. The lattice has a characteristic density $\gamma \in (0,1)$ defined as the scatterer diameter γb normalized by the linear unit-cell dimensions b. Our study will be restricted to two dimensions, enabling the unit-cell shape to be characterized by a single angle ψ once the cell lengths have been normalized to unity. The *system* consists of either a single point-sized particle or a noninteracting ensemble of particles, each interacting only with the Galton board and each moving under the influence of a constant gravitational acceleration **g**, where β is the angle of this vector from the horizontal. The interaction between particles and scatterers is inelastic in general and is quantified by a restitution coefficient $e \in [0,1]$ in a direction normal to the scatterer surface.

Heretofore, analysis of Galton boards [3,4] have been limited to the purely elastic case. However, by energy-conservation constraints, this case cannot approach an attractor in phase space. Consequently, Newtonian mechanics is abandoned in such analyses in favor of isokinetic mechanics. We address the energy problem in a more intuitive way by introducing inelasticities in interactions between particles and scatterers. Additionally, existing analyses do not provide a comprehensive study of parameter variations, an identification of sources of instability and indeterminism, or general criteria for the presence of anomalous behavior. We will deal with each of these matters.

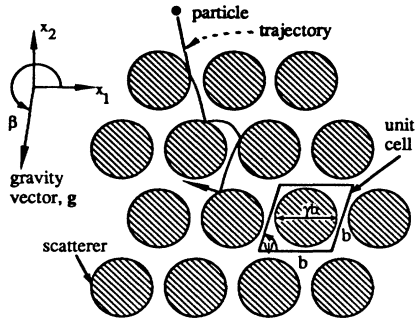

FIG. 1. Particle falling through a spatially periodic array of rigid scatterers. Gravity drives the particle's motion through the lattice at an angle β from the x_1 axis. The x_2 axis is perpendicular to the x_1 axis. The unit cell for the lattice is a rhombus with sides of length b, where one pair of sides is parallel to the x_1 axis and the other makes an angle ψ from the x_1 axis. Collisions occur off scatterers whose restitution coefficient is e and diameter is γb. The scatter's center is at the center of the rhombus, lying at the point of intersection of the two diagonals.

The Lorentz gas, which has been studied extensively [5–15], is identical to a purely elastic Galton board when gravity is absent. Consequently, results ascertained from the analysis of Lorentz gases has relevance to the present work. Seminal work by Sinai [5] established that Lorentz gases are ergodic and K systems. Analytic arguments along these lines were continued into the 1970s [6–8]. More recently, Lorentz gases have been the subject of numerous numerical simulations [9–15]. Apart from being restricted geometrically, these tend to be focused on the evolution of velocity autocorrelation functions. We will not employ these functions in the ensuing study. We find that the information concerning bifurcations in phase space and desired statistical quantities are more easily obtained from other sources.

The bouncing-ball problem [16–21], in which a ball collides inelastically with a sinusoidally moving table, has elements in common with the Galton board problem. Moreover, the bouncing-ball problem is far simpler mathematically. Bifurcations from periodic to chaotic behavior are observed [16]. Smale horseshoes exist in certain parameter regimes. Such behavior may carry over into Galton boards.

While integrating aspects from both the Lorentz gas and the bouncing-ball problem, the Galton board possesses unique aspects absent from either. Therefore, accessing the Galton board's unique underlying structure will be essential to understanding its observed behavior. There is a difficulty, however, in doing so with any degree of mathematical rigor. As we shall see, the Galton-board phase space may be represented as a three-dimensional discontinuous map. Such systems are not completely understood from a dynamical systems point of view. Moreover, what is understood requires an explicit form for the map itself: something which is difficult to come by for the Galton-board system. Additionally, many proofs require *a priori* existence of well-defined structures such as periodic cycles or homoclinic orbits. The only practical means (that the authors are aware of) by which such objects can be known to exist for certain are numerical.

Therefore, we will not make an attempt for mathematical rigor in this paper. Rather we will make an appeal to geometric and physical considerations to ascertain qualitative properties of the system, while supplementing such analysis with explicit numerical simulations of the system. In Sec. II, we begin by investigating the details of trajectory evolution. Issues concerning trajectory stability and attracting domains are treated therein. In Sec. III, we identify possible characteristics of an attracting domain in phase space. A Poincaré section is defined and a mapping that characterizes Galton-board dynamics is constructed. Smale horseshoes appear in limiting cases; the presence of strange and periodic attractors in phase space is addressed. In Sec. IV, we furnish numerical results that complete the dynamical systems analysis by providing concrete examples of attracting behavior. Fi-

nally, in Sec. V, we present statistical observations based on numerical simulations. We focus therein on the presence and absence of random behavior in particular parameter regimes. Interesting exceptions to expected Galton-board behavior, characterized by a failure to provide a realization of the "laws of probability," are discussed.

II. PHASE FLOW DYNAMICS

In this section we wish to deal with the microscopic details of the system. Specifically, we wish to examine how trajectories behave in phase space. Three topics are of particular interest: behavior of trajectories during collision, stability of trajectory evolution, and existence of regions of attraction. We begin by examining the ordinary differential equation (ODE) set that governs system behavior.

A. The ODE system

The equations describing Galton-board systems may be formulated as the dynamical system

$$\begin{aligned}\frac{d\mathbf{x}}{dt}&=\mathbf{v}\ ,\\ \frac{d\mathbf{v}}{dt}&=\mathbf{g}+\boldsymbol{\delta}_c(\mathbf{x},\mathbf{v};\gamma,e,\psi)\ ,\end{aligned}\tag{1}$$

where $\mathbf{g}$ is the constant gravitational acceleration vector ($\mathbf{g}=g\mathbf{g}^*$) of magnitude $g=|\mathbf{g}|$ and $\boldsymbol{\delta}_c$ is the impulsive collision acceleration vector ($\boldsymbol{\delta}_c=g\boldsymbol{\delta}_c^*$). The functional dependence of $\boldsymbol{\delta}_c$ on the position vector $\mathbf{x}$ of the particle is manifested through the parameters γ and ψ characterizing the lattice geometry; its dependence on the velocity vector $\mathbf{v}$ is manifested through e, the restitution coefficient. One can nondimensionalize the system (1) such that no scale-dependent parameters remain:

$$\mathbf{x}^*=\frac{\mathbf{x}}{b}\ ,\quad \mathbf{v}^*=\frac{\mathbf{v}}{\sqrt{gb}}\ ,\quad t^*=t\sqrt{g/b}\ .\tag{2}$$

Upon incorporating this normalization, the dynamical system equations of particle motion adopt the form

$$\begin{aligned}\frac{d\mathbf{x}^*}{dt^*}&=\mathbf{v}^*\ ,\\ \frac{d\mathbf{v}^*}{dt^*}&=\mathbf{g}^*+\boldsymbol{\delta}_c^*(\mathbf{x}^*,\mathbf{v}^*;\gamma,e,\psi)\ .\end{aligned}\tag{3}$$

Accordingly, the system is completely characterized by three phase variables (t^*,$\mathbf{x}^*$, and $\mathbf{v}^*$) and four characteristic parameters (γ, e, β, and ψ).

The system behavior will be investigated as these four parameters are varied. In this context, the ordinary differential equation system (3) proves to be inconvenient. All interesting dynamics is condensed into the collision term which—being impulsive—is not well characterized as an acceleration. This collision term is more suitably employed in an algorithm for computing individual trajectories (cf. the collision equations derived later in this section). A geometric analysis appealing to this algorithm will be used for system study. The system (3) will be used only as a formal guideline for studying the dynamical systems behavior of the Galton board.

As the scattering lattice is periodic in position space, so too must be the impulsive collision acceleration term. As such, position space may be represented as a unit cell or torus, whence the phase space is homeomorphic to $T^2\otimes\mathbb{R}^2$ with the real plane constituting velocity space. There exists only one scatterer in toroidal phase space. A typical trajectory winds around the torus while moving with constant speed in velocity space along the direction of gravity. Eventually the trajectory encounters the scatterer, whereupon the velocity is reoriented. The trajectory then continues as before until the next encounter, and so on.

There is only one fixed point in phase space, namely the point on the scatterer surface whose normal points in a direction directly opposite to that of gravity. Since the scatterer is convex, this point is unique and hyperbolically unstable. Small displacements to the left or right cause the particle to move away from the fixed point. Displacements opposite to gravity cause the particle to bounce repeatedly on the surface until dissipation brings the particle to rest at the fixed point. The presence of this point may generate indeterminacy in the system's behavior since there may exist homoclinic orbits connecting the fixed point to itself. Chaotic behavior will be addressed later, after the machinery needed to deal with such an issue is in place. The fixed point represents rather trivial dynamics at this point. Understanding more interesting phase flow behavior requires an investigation of the reorientation process associated with a collision. Accordingly, in what follows, we examine the dynamical consequences stemming from a particle colliding with a rigid surface.

B. Collision relations

Let three parameters, namely θ,φ,v, be specified for a particle incident to collision, as depicted in Fig. 2. The two post-collisional parameters v' and φ' are computed assuming inelastic rebound from a frictionless scattering surface. These latter parameters may be evaluated via an algorithm summarized in Fig. 3. First, imagine that Fig.

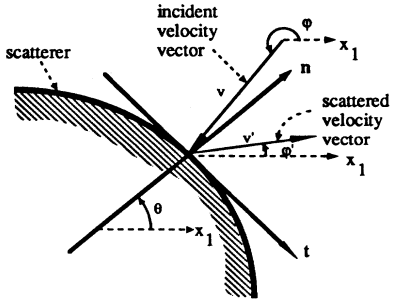

FIG. 2. Particle colliding with a scatterer. An incident velocity vector with magnitude $v=|\mathbf{v}|$ and incidence angle φ from the x_1 axis is scattered off a surface whose unit outward normal $\mathbf{n}$ is at an angle θ from the x_1 axis. The vector is redirected with magnitude v', making an angle φ' relative to the x_1 axis.

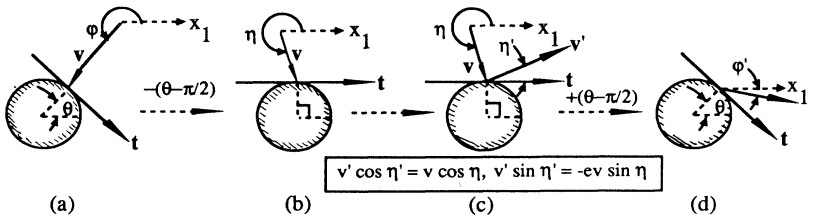

FIG. 3. Computation of collisional changes. (a) This figure is identical to Fig. 2. (b) Figure 2 is rotated so that the tangent vector t to the scatterer is now pointing in the $+x_1$-axis direction. This serves to define the angle η. (c) The new velocity vector is computed such that the component normal to the surface is $-e$ times the original, whereas the component tangential to the surface remains unaffected. (d) Finally, the tangent vector is rotated back to its original orientation.

3(a), which is identical to Fig. 2, is rotated such that the tangent to the scatterer points in the x_1 direction. Next, the collision algorithm is applied. Finally, the system is returned to its original orientation, Fig. 3(d). The new velocity vector has magnitude v' and makes an angle φ' with the x_1 axis.

Given an incident velocity vector in an arbitrary direction, its new direction following scattering can only adopt particular values, depending on the parameters assigned. Assume $\varphi=0$ for simplicity; no generality is lost since the reference direction can always be rotated. Begin with incidence angles θ varying from $-\pi/2$ to $\pi/2$. The boxed equations shown in Fig. 3 demand that since $\eta=\pi/2-\theta$,

$$v'\cos\eta'=v\cos(\pi/2-\theta)\equiv v\sin\theta\ ,$$

$$v'\sin\eta'=-ev\sin(\pi/2-\theta)\equiv -ev\cos\theta\ .$$

But, from trigonometric identities,

$$v'\cos\eta'=v'\cos(\pi/2-\theta+\varphi')$$

$$=v'(\sin\theta\cos\varphi'-\cos\theta\sin\varphi')$$

$$\therefore v'\cos\eta'=v_1'\sin\theta-v_2'\cos\theta\ ,$$

$$v'\sin\eta'=v'\sin(\pi/2-\theta+\varphi')$$

$$=v'(\cos\theta\cos\varphi'+\sin\theta\sin\varphi')$$

$$\therefore v'\sin\eta'=v_1'\cos\theta+v_2'\sin\theta\ .$$

Therefore,

$$v\sin\theta=v_1'\sin\theta-v_2'\cos\theta\ ,$$

$$-ev\cos\theta=v_1'\cos\theta+v_2'\sin\theta\ ,$$

whence

$$(v-v_1')\tan\theta=-v_2'\ ,$$

$$ev+v_1'=-v_2'\tan\theta\ .$$

These combine to yield

$$(v-v_1')(ev+v_1')=v_2'^2\ .$$

Consequently, we achieve the desired relation

$$\left[v_1'+\frac{e-1}{2}v\right]^2+v_2'^2=\left[\frac{e+1}{2}v\right]^2\ , \tag{4}$$

relating the incident and recoil velocity vectors.

Equation (4) suggests that, for a specified incident velocity vector $\mathbf{v}$, the allowed recoil velocity vectors $\mathbf{v}'$ form a circular locus in velocity space. The point where v' is greatest coincides with the $+\mathbf{v}$ direction, in which case $v'=v$. The $\mathbf{v}'$ locus near this point of maximum magnitude consists of those grazing trajectories arising from collisions occurring nearly tangent to the scatterer. The point where v' is smallest corresponds to the $-\mathbf{v}$ direction, for which circumstances $v'=ev$. The $\mathbf{v}'$ locus near this point of minimum magnitude consists of those trajectories arising from collisions occurring nearly normal to the scatterer. Note that $v'\leq v$ in all cases. This inequality suggests that collisions drive trajectories towards the velocity-space origin, an essential feature if attractive behavior is to exist.

In what follows, we will often examine trajectories in velocity-space projections of phase space, permitting us to take advantage of two-dimensional space visualization over that of four-dimensional space. Figure 4 exhibits a typical phase trajectory when projected onto velocity space. This visual aid will later be used to envision attracting regions in phase space, as well as to rationalize particular details of the Poincaré map.

C. Trajectory stability

Trajectory stability proves critical in identifying chaotic or regular attractors in phase space. Consider two proximate phase points whose coordinates are $(\mathbf{x},\mathbf{v})$ and $(\mathbf{x}+\Delta\mathbf{x},\mathbf{v}+\Delta\mathbf{v})$, respectively. Let both points evolve during the free-fall process prior to collision: their behavior under collision will be investigated later. Since, between collisions, both particles accelerate at identical rates, $d(\Delta\mathbf{v})/dt=\mathbf{0}$. Hence no divergence or convergence in velocity space is expected while both particles undergo free fall. Integration of the identity $d(\Delta\mathbf{x})/dt=\Delta\mathbf{v}$ reveals that $\Delta\mathbf{x}(t)=(\Delta\mathbf{v})t+\Delta\mathbf{x}_0$, where $\Delta\mathbf{x}_0$ denotes the position-space separation at time $t=0$. Given sufficient time during free fall, $|\Delta\mathbf{x}|$ diverges [22]. Once $|\Delta\mathbf{x}|\approx 1$, the two trajectories have moved into different regions on the torus representing position space, and the trajectories have thus effectively decorrelated during the free fall.

Consider the behavior during collision of two close trajectories characterized by (θ,φ,v) and $(\theta+\Delta\theta,\varphi+\Delta\varphi,v+\Delta v)$, respectively. In such circumstances, upon defining

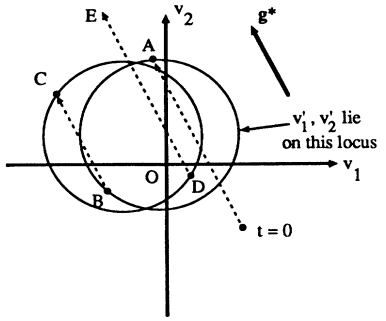

FIG. 4. Trajectory in velocity space. At $t=0$ the trajectory starts at some arbitrary point. It increases at a constant rate in the direction of gravity $\mathbf{g}^*$ until a collision occurs at A. The recoil velocity lies somewhere on a circle passing through A; where specifically on the circle this occurs depends upon the position on the scatterer at which the collision occurred. Suppose that the new velocity is situated at B. Gravitational effects resume until another collision occurs at C. The process repeats itself following each collision.

$$\eta=\varphi-\theta+\pi/2 ,$$

we find that

$$\eta+\Delta\eta=(\varphi+\Delta\varphi)-(\theta+\Delta\theta)+\pi/2 ,$$

whence

$$\Delta\eta=\Delta\varphi-\Delta\theta .$$

In turn, from the boxed equations in Fig. 3,

$$(v'+\Delta v')\cos(\eta'+\Delta\eta')=(v+\Delta v)\cos(\eta+\Delta\eta) ,$$

$$(v'+\Delta v')\sin(\eta'+\Delta\eta')=-e(v+\Delta v)\sin(\eta+\Delta\eta) ,$$

requiring that

$$\tan(\eta'+\Delta\eta')=-e\tan(\eta+\Delta\eta) ,$$

$$\tan\eta'+\Delta\eta'\sec^2\eta'=-e[\tan\eta+\Delta\eta\sec^2\eta] .$$

Employing the boxed equations in Fig. 3, the latter equation implies

$$\Delta\eta'=-e\Delta\eta\frac{\cos^2\eta'}{\cos^2\eta} .$$

Consequently,

$$\Delta\varphi'=\Delta\theta-e(\Delta\varphi-\Delta\theta)\frac{\cos^2\eta'}{\cos^2\eta} ,$$

or, equivalently,

$$\Delta\varphi'=\Delta\theta-e(\Delta\varphi-\Delta\theta)\frac{v^2}{v'^2} . \tag{5}$$

In reference to the preceding equations, one may always define $\Delta\theta$ so as to satisfy the inequality $\Delta\theta>0$. When $e=1$, it follows that $v'=v$, whence $|\Delta\varphi'|\geq|\Delta\varphi|$ if $\Delta\varphi\leq 0$, i.e., when trajectories point away from each other. The scatterer convexity thus causes a divergence between proximate velocity vectors in this perfectly elastic case. However, when $e<1$, nothing can be said about whether $\Delta\varphi'$ is larger or smaller than $\Delta\varphi$. With smaller e, the pre-collision parameter $\Delta\varphi$ becomes less significant. Indeed, when $e=0$, $\Delta\varphi'$ depends only on $\Delta\theta$. Differences between trajectories are mollified upon collision when interactions between particle and scatterer are inelastic. Hence there exists a balance between competing effects, namely, scatterer convexity enhances the divergence of initially close trajectories, whereas scatterer inelasticity enhances their convergence. As inelasticity was previously observed to drive such trajectories closer to the velocity-space origin, inelasticity also contributes to trajectory stability as embodied by convergence.

D. Regions of attraction

We wish to identify whether there exist regions where trajectories converge. To do this, we will examine the nature of trajectories that are divergent in phase space. It is useful to consider the Galton-board phase space to be imbedded in the phase space of another system, viz. the dissipative Lorentz gas. This imbedding leads to important conclusions concerning the behavior of possibly divergent trajectories in phase space.

Since the only way in which a trajectory can be unbounded is to go out to an infinite velocity magnitude, we wish to study trajectory behavior as $v\rightarrow\infty$. But recall that at large v, gravity is for the most part negligible. The system may be treated as a dissipative Lorentz gas (DLG). In effect we can envision the phase space of the Galton board as being imbedded in the phase space of a DLG. But the attractor for the DLG is trivial; it is the origin. Particles in the lattice eventually lose all their energy and come to rest asymptotically. Interestingly enough, the DLG phase space is identical for arbitrary scalings in the v direction, i.e., the dynamics of a DLG are independent of the velocity magnitude. This statement can be deduced from discussion concerning collision relations in Sec. II B.

However, one cannot draw an immediate conclusion about an attractor in Galton-board phase space from the above considerations. Two points are important to note: First, as a trajectory approaches the origin, gravity becomes increasingly important, leaving the DLG approximation increasingly suspect. Second, the perturbative effect of gravity, even in the DLG limit, can effect an energy increase between collisions that challenge the existence of a definitive bounding velocity.

Before embarking on the characterization of the DLG limit, we introduce a function that will help characterize the lattice. We define $\lambda(\theta,\mathbf{n})$ to be the length of a line segment attached to a scatterer at θ and pointing in the $\mathbf{n}$ direction. The line segment terminates at the next scatterer encountered. $\lambda(\theta,\mathbf{n})$, therefore, is the free path of a particle in a DLG. Note that $\lambda(\theta,\mathbf{n})$ will be finite for a finite scatterer diameter.

Let us now identify at what v gravity is negligible. Consider a typical $\mathbf{r}(t)$ between collisions. Under the influence of gravity,

$$\mathbf{r}(t)=\mathbf{v}_0t+\tfrac{1}{2}\mathbf{g}t^2 , \quad \mathbf{v}(t)=\mathbf{v}_0+\mathbf{g}t ,$$

where the origin of the coordinate system is at the initial point on the scatterer. Let T be the time at which the particle collides, with the next scatterer for the actual system. Let T_0 be the time at which the particle collides with the scatterer for the DLG approximation. Consider the system close enough to a DLG that both the particle for the actual system and that for the approximation collide with the same scatterer. The difference between T and T_0 will clearly be small.

We wish to find the difference $\mathbf{r}(T)-\mathbf{r}(T_0)$. When gravitation is negligible, the magnitude of this quantity will be small compared with the magnitude of $\mathbf{r}(T_0)$. Consider the following Taylor expansion:

$$\mathbf{r}(T)=\mathbf{r}(T_0)+[T-T_0]\mathbf{v}(T_0)+\tfrac{1}{2}[T-T_0]^2\mathbf{g}+O([T-T_0]^3) .$$

Using the relations $\mathbf{r}(T_0)=\mathbf{v}_0T_0+\mathbf{g}T_0^2/2$ and $\mathbf{r}_0(T_0)=\mathbf{v}_0T_0$, we get finally

$$\mathbf{r}(T)-\mathbf{r}_0(T_0)=\tfrac{1}{2}\mathbf{g}T_0^2+[T-T_0]\mathbf{v}(T_0)+\tfrac{1}{2}[T-T_0]^2\mathbf{g}+O([T-T_0]^3) .$$

We want this quantity to be small relative to the magnitude of $\mathbf{r}(T_0)$. We wish to set v_0 to some large value. But in this case, the terms in the previous equation containing $T-T_0$ should go to zero. Therefore, we choose

$$\tfrac{1}{2}gT_0^2=\epsilon r_0(T_0) ,$$

$$\frac{1}{2}g\left[\frac{r_0(T_0)}{v_0}\right]^2=\epsilon r_0(T_0) ,$$

where ϵ is a small number. But recognize that $r_0(T_0)$ is none other than $\lambda(\theta,\mathbf{n})$. Substituting and rearranging terms yield the following requirement for the neglect of gravity:

$$v_0^2=\frac{1}{2\epsilon}g\lambda(\theta,\hat{\mathbf{n}}) , \tag{6}$$

where, once again, ϵ is a small number. Therefore, so long as condition (6) is satisfied, trajectories will converge onto the origin, i.e., $v_{\text{new}}\le v_{\text{old}}$. This is a consequence of the DLG limit. This statement is not quite true, however. There will be a fraction of trajectories that will increase in v between collisions. This leakage of trajectories exists as a result of the unavoidable perturbative effect of gravity. Let us estimate this fraction. From Fig. 5, one can see that the following relation must hold:

$$v^2=\left[\frac{1-e}{2}\right]^2v'^2+\left[\frac{1+e}{2}\right]^2v'^2-2v'^2\frac{(1-e)(1+e)}{4}\cos(\pi-\varphi) ,$$

$$\frac{v^2}{v'^2}=\frac{1+e^2}{2}+\frac{1-e^2}{2}\cos\varphi .$$

But we know the relation between v' and v:

$$\mathbf{v}'=\mathbf{v}+\mathbf{g}t ,$$

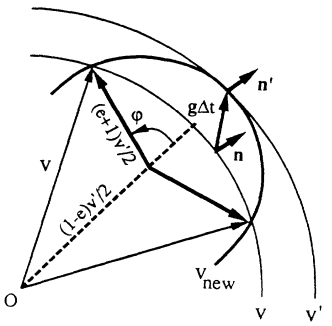

FIG. 5. Leakage from the attracting region. Gravitation carries the system from point A to point B (cf. Fig. 4). The emboldened arc is the circular locus representing the redirected velocity vector of those trajectories which are incident to a scatterer at point B. In the DLG limiting case, $\mathbf{n}$ and $\mathbf{n}'$ are almost identical.

$$\mathbf{v}'\approx v\left[\hat{\mathbf{n}}+\mathbf{g}^*\frac{g\lambda(\theta,\hat{\mathbf{n}})}{v^2}\right] ,$$

$$\hat{\mathbf{n}}\cdot\mathbf{v}'\approx v'\approx v\left[1+\hat{\mathbf{n}}\cdot\mathbf{g}^*\frac{g\lambda(\theta,\hat{\mathbf{n}})}{v^2}\right] ,$$

$$\frac{v'}{v}\approx 1+2\epsilon(\hat{\mathbf{n}}\cdot\mathbf{g}^*) .$$

Substituting into the law of cosines relation and noting that φ is a small angle,

$$1-4\epsilon(\hat{\mathbf{n}}\cdot\mathbf{g}^*)+O(\epsilon^2)\approx 1-\frac{1-e^2}{4}\varphi^2+O(\varphi^4) .$$

Therefore, the fraction F of trajectories that increase in energy between collisions for a given ϵ is

$$F\approx\frac{2\varphi}{2\pi}\approx\epsilon^{1/2}\frac{4}{\pi}\left[\frac{\hat{\mathbf{n}}\cdot\mathbf{g}^*}{1-e^2}\right]^{1/2} .$$

Therefore, so long as v is on the manifold as designated by Eq. (6), where v_0 is replaced by v, the energy will decrease between collisions (including redirection) with the exception of a fraction of trajectories proportional to $\epsilon^{1/2}$ when $v\sim\epsilon^{-1/2}$ and ϵ is a small number. Note that this fraction of trajectories are those trajectories that collide nearly tangent to the scatterer as suggested by Fig. 5. There appears to exist an asymptotic bounding of phase-space trajectories We can therefore expect there to exist an attractor in the phase space of the Galton-board system.

Note that the bound placed on the attracting region as specified by Eq. (6) may be greatly improved in portions of phase space where the direction of velocity is opposite that of gravity. In such regions, gravitation itself causes v to decrease between collisions so long as

$$v\ge\frac{g\Delta t}{|\hat{\mathbf{n}}\cdot\mathbf{g}^*|} , \tag{6'}$$

where Δt is the time between collisions. This condition ensures that v is not so small as to start increasing from

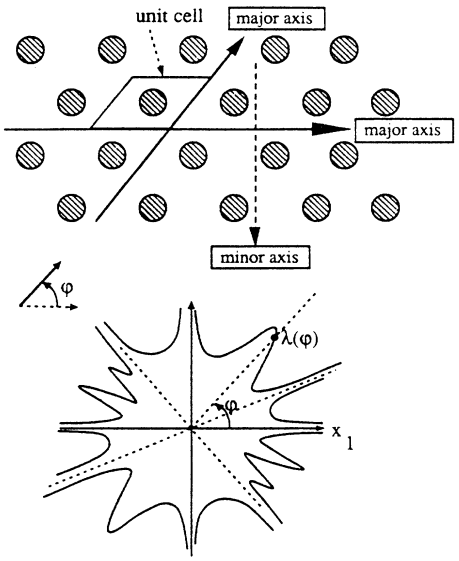

FIG. 6. Typical behavior of $\lambda(\theta,\mathbf{n})$ and major and minor axes. Since the system is in two dimensions, $\mathbf{n}$ may be represented by a single angle φ. Note that λ will vary with changing θ, but the velocity dependence is most relevant here. The directions close to the unit-cell directions, and where λ is large, are termed the *major axes*. The other directions with large free path will be termed the *minor axes*.

gravity's effect.

When λ becomes very large, the attractor may reach out into large energy regions. In the way we defined the lattice, directions close to the directions used to define the unit-cell rhombus will have large λ. Let us call any direction with large λ a *lattice axis*. Moreover, those lattice axes which are associated with the unit-cell directions will be called *major axes*. All other lattice axes will be designated *minor axes*. Figure 6 schematically depicts λ for a typical lattice. We will see later that these axes play a role in determining the behavior of attracting sets.

To summarize, a combination of two effects is shown to exist, namely attraction to a bounded domain and loss of initial information. Both suggest the existence of an attractor in phase space. Moreover, the general criteria for trajectory stability suggest under what parameter ranges an attractor is periodic or strange. The more trajectories are stable, the more likely the attractor is periodic or quasiperiodic. Conversely, the more trajectories are unstable, the more likely the attractor is chaotic. Additional features of the attractor's characteristics may be extracted from a particular Poincaré map.

III. POINCARÉ MAP DYNAMICS

A. The Poincaré section

Choose a Poincaré section at the scatterer surface and plot points in phase space at times such as A and C in Fig. 4. One could also take points at B and D, but the former selection is more revealing. The remainder of the trajectory is unenlightening and, indeed, obfuscates important behavior when projected onto velocity space. The Poincaré section reduces the number of interesting phase-space dimensions to three, the two velocity-space dimensions plus an angle representing the point on the scatterer surface at which the collision occurs. Consequently, the Poincaré section, hereafter referred to as Σ, is homeomorphic to $S^1 \otimes \mathbb{R}^2$. Since the scatterer is convex, there exists a unique value of θ for every point lying upon the surface. Figure 2 physically depicts the three Σ variables, namely v, φ, and θ.

The Poincaré section shown in Fig. 7 possesses several notable features. First, all points occupy only half of Σ since $\mathbf{n}\cdot\mathbf{v} \leq 0$, where $\mathbf{n}$ is the unit outward normal to the scatterer at θ, as in Fig. 2. The helicoid that represents the boundary between the two halves represents the locus $\mathbf{n}\cdot\mathbf{v}=0$, its axis corresponding to the line $\mathbf{v}=\mathbf{0}$. The fixed point lies on this surface along the axis $\mathbf{v}=\mathbf{0}$ at $\theta=\theta_0$. There exists a surface in Fig. 7 running through the vertical line intersecting the fixed point. The surface represents those points that are unstable under small displacements. Note that this surface includes all points that eventually map onto the fixed point. More importantly, it includes all high-velocity trajectories that are incident normal to the scatterer. One can see this to be the case when one considers the DLG limit [23]. This surface will be referred to as the *hyperbolic* boundary since those points in Σ which lie to one side of the surface map in a particular direction, whereas those points on the other side map in the opposite direction. The hyperbolic boundary does not generally partition the region bounded

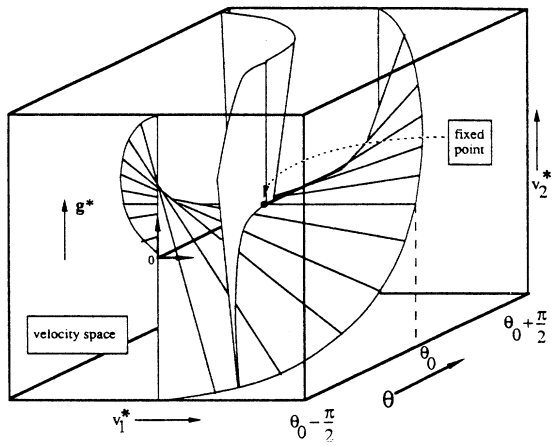

FIG. 7. The Poincaré section. Velocity space is represented by the face parallel to the plane of the paper, with θ the depth. The helicoid is the manifold representing the locus of trajectories that collide tangentially with the scatterer. Since only incident trajectories are represented, all points in Σ must lie above this surface. The fixed point is located at $\mathbf{v}=\mathbf{0}$ and $\theta=\theta_0$. Relative to the helicoid's orientation, gravity points upward. The manifold running through the vertical line emanating from the fixed point consists of those points which eventually map onto the fixed point. For clarity, the section where $\theta \in (\theta_0+\pi/2, \theta_0+3\pi/2)$ is not shown.

by the helicoid. One can envision a special case of this manifold by considering all those particles that bounce repeatedly on the fixed point until they come to rest. Any particles with momentum to the left will scatter to the left, whereas those with momentum to the right will scatter to the right.

The Poincaré map f: $\Sigma \rightarrow \Sigma$ takes those elements representing the state of the system at incidence and maps them into those subsequent system states corresponding to incidence at the *next* collision. This is a closed map for all Σ, except that subset of Σ possessing relative measure zero, the latter representing states which do not subsequently collide with any scatterers. One can incorporate the graphical algorithm depicted in Fig. 4 to show how the map affects Σ. Now, however, the circular locus in $\mathbf{v}$ space is a projection of an arc in Σ possessing a unique $\mathbf{v}$ for a given θ. Gravity's effect on system evolution is identical to that represented in Fig. 4, except that the new θ appropriate to the next collision is uniquely determined; the particular value that θ adopts depends upon the map's details.

B. Unit cell partitions of Σ

The map f partitions Σ into disjoint regions $\{P\}$, such that all elements in each region collide with a scatterer in a particular unit cell. Figure 8 depicts several illustrative trajectories. Each point in Σ (except for those few which do not collide with scatterers) lies in exactly one region P. Boundaries between regions possess the following interpretation: if a point in Σ lies on a boundary, it collides tangentially with a scatterer, as depicted by those trajectories in the upper-left-hand corner of Fig. 8. All particles represented by interior points do *not* collide tangentially with a scatterer, but rather collide such that a nonzero change in velocity occurs. The partition then may be described as a primary unit-cell partition; given any point in Σ, the partition determines the next unit cell within which the collision occurs. The partition is nothing more than the inverse mapping of the helicoid representing the locus $\mathbf{n}\cdot\mathbf{v}=0$. Trajectories appearing in the lower-right-hand corner of Fig. 8 suggest that a boundary maps into *two* marginally decorrelated regions. A trajectory close to a boundary is unstable to some degree. More importantly, however, is the fact that each region P has the possibility of containing some portion of the hyperbolic boundary. If so, trajectories on opposite sides of that surface become completely decorrelated.

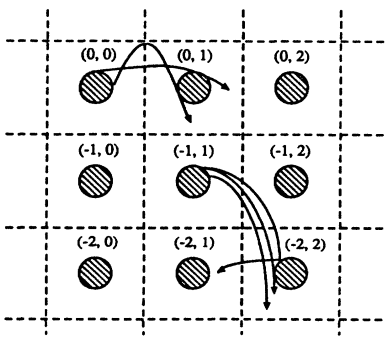

FIG. 8. Unit cell partition. Two trajectories originating within the same unit cell (0,0), and colliding in the same unit cell (m,n), are assigned to the same region P in the unit cell partition.

The process can be repeated. If f represents the map, then f: $\Sigma \rightarrow \Sigma$ is a function such that $P \rightarrow Q \subset \Sigma$. If Q contains boundaries from the primary partition, then following the second collision, P partitions into two or more regions. The process repeats itself. Each $P \subset \Sigma$ can be partitioned into regions which remain within the same unit cell after two collisions. Call these smaller regions P'. One can then partition P' into still smaller regions P'', which remain within the same unit cell after *three* collisions, and so on.

Consider a general unit cell partition constructed over an *infinite number* of collisions. Since all trajectories approach the region near the velocity-space origin as indicated in Sec. II D, and since boundaries do not map into themselves in general [24], there necessarily exist an infinite number of boundaries lying within the finite domain defined by the attractor. Hence regions densely populated with boundaries coexist with those possessing no boundaries at all. These open (boundary-less) regions must map into one another, for if they mapped into regions with boundaries, the regions themselves would contain boundaries—a contradiction.

Consider those regions densely populated with boundaries. Recall that the partition boundaries correspond to tangential collisions, whence regions densely populated with partition boundaries possess high-energy trajectories. Physically, it can be seen that these high-energy trajectories occur in lattice-axis directions proximate to the direction of gravity. But at higher energies, the hyperbolic boundary tends to be relatively exposed in each region of the unit cell partition. Therefore, decorrelation occurs in regions highly populated with partition boundaries. In general, the hyperbolic boundary may possibly be encountered within *every* region enclosed by partition boundaries. However, the hyperbolic boundary may also be shielded by other scatterers. Which scenario actually occurs depends strongly on the map itself. Consequently, the system's description is incomplete without a more detailed description of the mapping.

Given the above situation as restricted by geometric and physical considerations, only a few scenarios seem to be possible.

(i) The attractor is dense with partition boundaries and hyperbolic boundaries (i.e., all trajectories decorrelate). High-energy dissipative chaos exists exclusively.

(ii) The attractor is dense with hyperbolic boundaries, but not with partition boundaries. Low-energy dissipative chaos exists.

(iii) The attractor is not dense with hyperbolic boundaries. All trajectories eventually map into open regions which map into themselves, i.e., trajectories avoid partition and hyperbolic boundaries (by definition of open regions). The attractor will be contained within the open regions. Stable periodic or quasiperiodic cycles exist, but with chaotic transients.

(iv) A combination of the above cases exists with disjoint basins of attraction.

C. The limiting case $\gamma \to 0$

As γ approaches zero, the time interval between successive collisions becomes very large and velocities become aligned with gravity. Owing to this large mean free path, most trajectories are dominated by gravitational rather than collisional influences. If v should become so large as to not be significantly affected by gravity, the particle suffers a collision and hence becomes more susceptible to gravity after a time $t \approx \tilde{\lambda}/v$. The resulting situation is depicted in Fig. 9.

For $\Delta \mathbf{v} \neq \mathbf{0}$, initially small differences in $\Delta \mathbf{x}$ grow as the trajectories evolve. Since all trajectories align, all points of Σ lying in a particular region P of the primary unit-cell partition can possess only small velocity differences $\Delta \mathbf{v}_0$. Indeed, if $\tilde{\lambda} \approx gt^2/2$, then $t \approx (2\tilde{\lambda}/g)^{1/2}$ constitutes the nominal time between collisions. But $\Delta \mathbf{x} \approx (\Delta \mathbf{v})t$, although the maximum allowable $|\Delta \mathbf{x}|$ for two points to lie in the same region P is approximately γ. Hence the maximum allowable initial velocity difference between two points lying in the same region P is $|\Delta \mathbf{v}_0| = |\Delta \mathbf{v}| \approx \gamma/t$ — a small quantity. Thus the fraction of Σ occupied by any one region P is very small. But, the *scattered* velocity vector occupies all the points on the circular locus, implying that a full 2π range of φ is covered by the map of the region P (this mapping corresponds to a mapping of each region P onto a region containing the hyperbolic boundary). Hence any $f(P)$ covers much more of Σ than any region P contained in the primary unit cell partition. Consequently, every region P is partitioned into multiple regions $P_i' = \{x \in \Sigma | f(x) \in P_i$ for some P_i in the primary unit cell partition$\}$, each containing the hyperbolic boundary. But since the new regions constituting P are merely smaller copies of portions of the original region, the new regions are themselves partitioned in the next level partition, and so on. Hence the entire attractor is dense with hyperbolic boundaries in the infinite collision partition. This implies all trajectories are unstable and yet remain within a confined region in phase space.

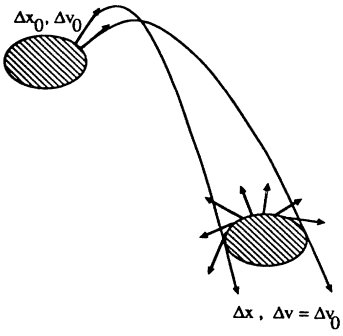

FIG. 9. Alignment of trajectories. Trajectories tend to align, given sufficient time to fall between successive collisions. Moreover, the fixed point is exposed to the trajectories. Hence scattering occurs in all directions.

Therefore, a strange attractor is present in the low-density limit.

We wish to ascertain the existence of a Smale horseshoe in Σ. Let us examine Σ in a more coarse way. In essence, upon each collision, a particle is scattered right or left. Then let a point in phase space be defined by a string of R's or L's where the nth character represents the direction of scattering upon the nth collision. Let us just examine the first collision. Σ is divided into two regions, either R_1 or L_1. Each of these regions is mapped onto Σ in such a way as to be partitioned by the boundary separating the original R_1 and L_1 regions. The second character in the string indicates which of these regions the original trajectory maps into.

Note that there is a one to one correspondence between the character strings and points in the Poincaré section. Moreover, by the nature of the Poincaré map, the evolution of a character string corresponding to a point in Σ is merely given by eliminating the first character and shifting each remaining character to the left. Employing arguments as outlined in Wiggins [25], a dynamical system given by this type of character string contains an invariant set which is dense in the Poincaré section and is sensitive to initial conditions. This invariant set is related to the set of irrational numbers in the set of real numbers. Moreover, this invariant set constitutes a Smale horseshoe.

Moreover, we see how this same argument applies even when the density is not strictly in the zero-density limit. So long as each region P is exposed to the hyperbolic boundary, the Smale horseshoe should exist. The conditions underlying such exposure require the presence of a low density (so that mean free path is sufficiently long) and a sufficiently high elasticity (so that the needed velocity transverse to gravity is provided). Strange attractors are expected to exist under these conditions.

D. The limiting case $e \to 1$

As guaranteed by the energy constraint, trajectories resulting in a zero terminal velocity are possible in the perfectly elastic case. Such trajectories either bounce on a single scatterer at the fixed point or bounce between a series of scatterers at more or less at the same potential energy. However, there exists numerical evidence that nonzero terminal velocities exist in perfectly elastic cases. Under such circumstances, one can show that an elastic system will exhibit chaotic behavior. This conclusion also follows from the energy constraint: If the system falls indefinitely through the lattice, it must acquire kinetic energy. Eventually, a regime is established in which gravitational effects on system behavior proves negligible, namely the Lorentz gas limit. In this context, it is well to recall from the analysis following Eq. (5) that when $e \to 1$, trajectories destabilize in the φ direction as well as in position space. Since energy is constant for the most part, trajectories diverge in the Lorentz gas limit. Moreover, the phase space for a Lorentz gas is compact as a consequence of the energy constraint. Hence chaos must ensue. One can think of the system as slowly migrating between shells of Lorentz gas behavior, each such shell suc-

cessively parametrizing a domain of increasing energy. A more precise argument for the existence of chaos in Lorentz gases is given by Sinai [5].

E. General observations

Since regions of Σ map into other parts of Σ, the attractor on Σ possesses a self-affine character associated with fractal sets. As discussed in Sec. II D, trajectories that lie close to partition boundaries constitute those trajectories that tend to increase in energy between collisions. Moreover, these densely boundaried regions exist in lattice-axis directions; consequently, border trajectories correspond to leakage from those high-energy regions that constitute the "fingers" of the attractor that reach into large-v regions along lattice-axis directions. Strange attractors and strange repellers dense with boundaries therefore tend to be high-energy attractors and repellers possessing the aforementioned characteristics. Moreover, periodic orbits tend to constitute low-energy phenomena, since they avoid partition boundaries. Ultimately, the existence of nontransient chaotic behavior requires the existence of a Smale horseshoe generated by homoclinic orbits.

Note that if lattice density is low, many unit cells are "visible" to particles in a particular unit cell. Therefore, the Poincaré section will be riddled with the partition boundaries. But as lattice density is increased, the scatterers in proximate unit cells will block more distant unit cells. There will exist fewer partition boundaries in the Poincaré section of such systems since the particles can only encounter a few different unit cells upon the next collision.

From the two special cases outlined above, one can construct a scenario for which strange attractors are unlikely to exist. In particular, such circumstances require: (a) restricting the mapping so that the hyperbolic boundary does not map onto itself and (b) maintaining low energies so that mappings onto the hyperbolic boundary from other regions are limited. These two criteria are achieved when the following criteria are met:

(i) Elasticity is low, so that a tendency exists for close trajectories to converge.

(ii) Lattice density is high, so that available boundaries are few, thereby mollifying the effects of convexity.

(iii) Trajectories avoid the fixed point, so that homoclinic orbits are not possible.

Unfortunately, the last condition is subtle since it depends upon the details of the Poincaré map. Indeed, the system's complexity will become manifest in Sec. IV when numerical simulations are presented. Ultimately, whether homoclinic or periodic orbits exist depends on the characteristics of the Poincaré map, which reflect the system's physical attributes. These special orbits dictate phase flow and, concomitantly, govern observed system behavior. The map is complex in general and sensitive to the details implicit in the governing equations. As a consequence, an appeal will be made to the detailed system dynamics via numerical solution of the governing equations over the parametric range of interest. These specific results will complement general results found in this section and Sec. II D.

IV. DYNAMICAL SYSTEMS RESULTS

A. Periodic attractors

Calculations reveal the existence of periodic orbits in Galton-board systems. Moreover, these orbits prove to be stable under numerical roundoff errors, time discretization, and applied perturbations. Additionally, most periodic states are observed to be parametrically robust. Periodic orbits occupy a significant fraction of parameter space; therefore, they may not be deemed pathological. Most importantly, the quantitative and qualitative effects of periodic systems on Galton-board behavior are drastic and are manifested even at statistical levels. This severely violates the conventional wisdom that Galton boards necessarily demonstrate random processes in nature.

The factors leading to stable orbits are many. First, inelasticity focuses close trajectories. Convexity's dispersing effect tends to be negated at lower elasticities. Second, high-lattice-density shields hyperbolic boundaries in the unit cell partition. Put more physically, the scatterers' close proximity to one another restricts the paths available to trajectories before the next collision. Third, high-lattice-density shortens the mean free path. The most important mode for decorrelating trajectories is the velocity difference $\Delta\mathbf{v}$; a finite value for this parameter causes trajectory divergence in $\mathbf{x}$ space [22]. However, the degree of such divergence is functionally dependent on time; thus, if the time between successive collisions is limited, the degree of possible divergence is correspondingly limited.

These factors provide a means by which partition boundaries and hyperbolic boundaries may be avoided. But a subtle balance exists between those forces which create divergence (hyperbolic points and boundaries in the unit-cell partition) and those which restrict divergence (inelasticity and lattice density). Given the system parameters, which of these factors dominates the system's ultimate behavior is not obvious. This is clear from the following investigation of parameter space.

Figures 10(a) and 10(b) show sample parameter spaces for hexagonal and square lattices, respectively. Figures 10(a i) and 10(b i) constitute parameter spaces for circumstances wherein gravity is directed along a *minor* lattice axis. In each consecutive figure, the gravity vector is rotated towards a major axis. Finally, Figs. 10(a vi) and 10(b vi) are parameter planes when gravity is directed along a *major* axis. Different periodicity regions represent different periodic orbit types. Figure 10 clearly reveals the complexity of the Galton board's bifurcation structure.

Periodic cycles occur in many different varieties. Most varieties are cycles that move along the major axis. Figure 11(a) shows the trajectory on the lattice for one such case. This figure may be visualized as if it were the Galton board itself, with the scatterers hidden. The tendency to move along a major axis is so strong that particles move in a direction significantly different from that of

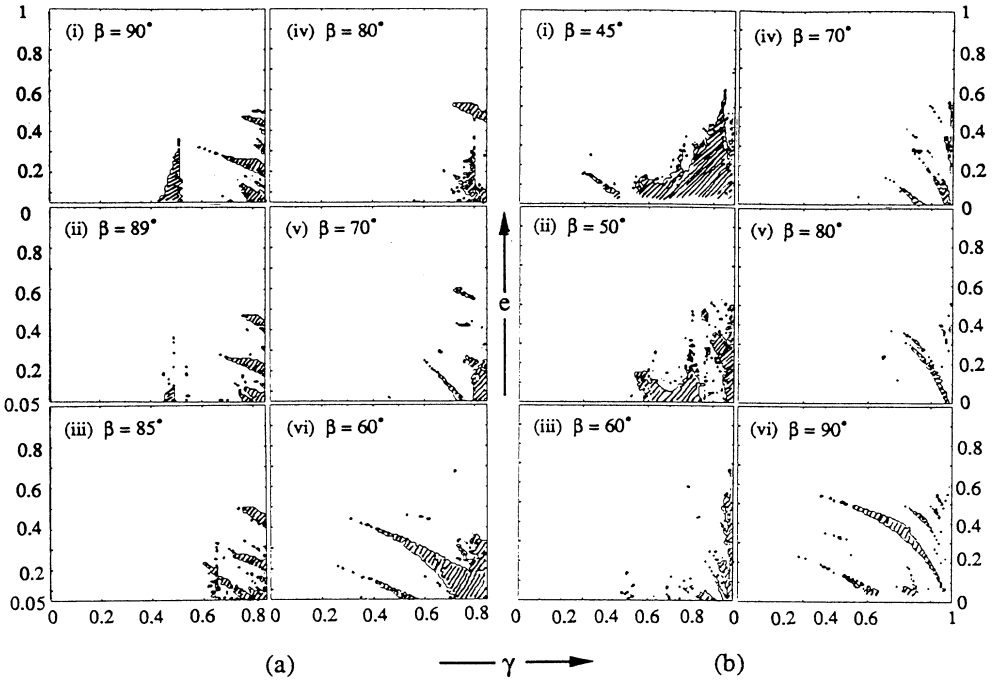

FIG. 10. (a) Parameter space for hexagonal lattice; (b) parameter space for square lattice. (a i) and (b i) represent parameter planes where gravity is oriented along a minor axis. (a vi) and (b vi) represent parameter planes where gravity is oriented along a major axis. The ordinate and abscissa correspond to e and γ, respectively. Periodic and quasiperiodic states are shown shaded; chaotic states are not. The algorithm used to generate these parameter spaces begins with allowing a trajectory from each case to stabilize. Then a small perturbation is added and the difference between the original trajectory and the perturbed trajectory is measured. If the difference remains small, the case is considered periodic or quasiperiodic. Conversely, if the difference explodes, the case is considered chaotic. Hence these diagrams distinguish cases where the Lyapunov exponents are respectively negative or positive.

gravity. This phenomenon will be seen later to also be manifested at the statistical level, when terminal velocities are discussed. The major-axis period cycles tend to occupy parameter space in tongues that stretch from high lattice density and low elasticity to low density and high elasticity. Figure 10 depicts many examples displaying this behavior. Since all cycles within a region of parameter space possess the same qualitative structure, the lower-density analogs have greater distances to traverse between scatterers than do their high-density cousins. As more transverse velocity is needed between collisions, more elasticity is needed to prevent degeneration of the orbit between scatterers caused by the pull of gravity.

The major-axis periodic cycles exhibit symmetry breaking when the gravity vector is rotated away from alignment with an axis possessing lattice symmetry to alignment with one devoid of such symmetry. Figure 11(b) represents a symmetric case that is broken into the two asymmetric cases shown in Fig. 11(c) when the gravity vector is rotated 5° away from the axis of symmetry. Note that the symmetry-broken cases follow major axes. This is true in general. Figure 10 reveals that periodic orbits are less prevalent in cases where gravity is not paral-

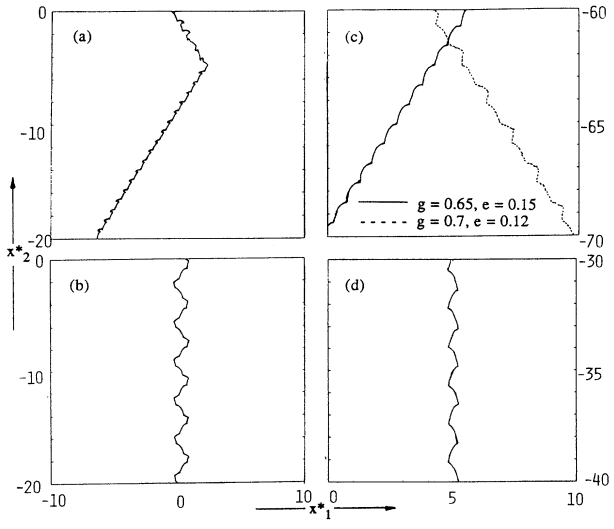

FIG. 11. Periodic cycles on the lattice. (a) Hexagonal lattice: $\beta=-90°, \gamma=0.8, e=0.46$. (b) Hexagonal lattice: $\beta=-90°$, $\gamma=0.85, e=0.05$. (c) Hexagonal lattice: $\beta=-85°$. (d) Hexagonal lattice: $\beta=-90°, \gamma=0.5, e=0.25$.

lel to an axis of lattice symmetry.

Minor-axis periodic cycles are structurally the simplest class of periodic cycles. They are fairly sensitive to gravity's direction relative to the lattice, and they tend to occur in circumstances for which the greatest symmetry exists. Figure 11(d) represents an example of such a periodic cycle on a Galton board. Figures 10(a i) and 10(b i) show the extent to which minor-axis periodicity exists for lattice configurations. Regions wherein these periodicities exist occupy triangular regions along the $e=0$ axis.

All periodic cases exhibit chaotic transients when initial energy is sufficiently large. Explicitly, strange repellers coexist in phase space with the stable periodic cycles. Figure 11(a) depicts a trajectory displaying a chaotic transient. Hence sensitivity to initial conditions may still exist in periodic systems. However, it is crucial to understand that such chaos is *not stable.* Over time, the trajectories stabilize into well-defined, well-behaved orbits. Moreover, no chaotic transient is observed if a low-energy initial condition is selected.

B. Bifurcations

The chaotic transients described above suggest a mechanism for the indeterminacy observed in physical situations. Initial energies in our numerical simulations tended to be rather large. The ensuing chaotic transient was consistent in qualitative structure with high-energy chaotic attractors, i.e., attractors dominated by partition boundaries. However, the chaotic transient eventually loses energy and stabilizes into a low-energy periodic attractor.

Figure 12 depicts a bifurcation from periodic to chaotic behavior when high-energy chaos exists. A low-energy periodicity explodes into a wildly erratic, high-energy chaotic attractor. More appropriately, the transient that precedes the periodicity gains more and more stability, while the periodic attractor loses stability. The transient ultimately becomes the attractor. Compare this bifurcation to the one exhibited in Fig. 13. As the bifurcation parameter is manipulated, the first periodicity loses sufficient energy to just encounter the fixed point. A crisis occurs: either the trajectory may continue along its major axis or it may shift into another major-axis periodicity. But the process repeats itself and an aperiodic, chaotic cycle is born from the homoclinic orbit connecting two crises. As the bifurcation parameter is manipulated further, the period between crises becomes sufficiently short that a new periodicity is generated from a combination of the two major-axis periodicities.

The dominant role played by major and minor axes is clear. These axes govern the existence of homoclinic orbits and dominate the directions which periodic orbits take. Therefore, these axes play a pivotal role in bifurcations. Hence, in addition to the effects of inelasticity and lattice density, the effects of lattice geometry are critical in ascertaining the qualitative nature of stable behavior.

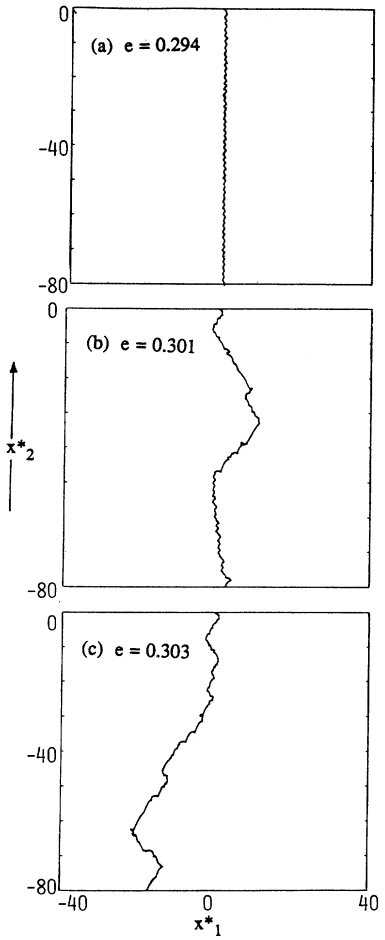

FIG. 12. Bifurcation on a hexagonal lattice. $\beta=-90°$, $\gamma=0.5$.

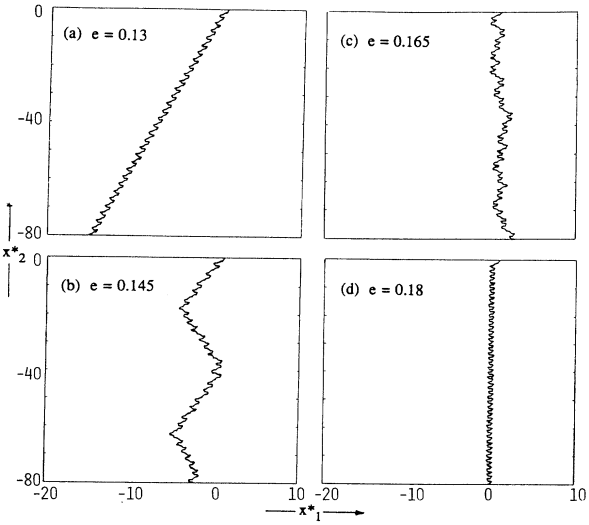

FIG. 13. Bifurcation on a hexagonal lattice. $\beta=-87°$, $\gamma=0.85$.

C. Strange attractors

Systems possessing chaotic attractors exist. Indeed, Fig. 10 clearly demonstrates that such systems dominate parameter space. Ultimately, strange attractors represent the classical random behavior ascribed to Galton boards. Higher elasticities and lower lattice densities yield chaotic steady states, consistent with results from preceding sections. Furthermore, when the gravity vector lacks lattice symmetry, chaotic cases are more prevalent. Figure 12(c) shows a typical chaotic trajectory. The erratic behavior expected is clear.

Figure 14 shows the attractors on the Poincaré map for several chaotic states. All cases exhibit a biasing in directions parallel to gravity. There also exists a diffuse texture to the generally featherlike structure. This diffusiveness is expected as a consequence of the leakage in phase space discussed in Sec. II D. Indeed, a few stray points occurring at very large v are not displayed in the figures. Figure 14(a) depicts a low-density attractor. Its self-affine structure is evident. Indeed, the base structure appears to consist of two arcs near $\mathbf{v}=\mathbf{0}$. This structure is most apparent in Fig. 14(b). The arcs represent low-velocity particles sliding off scatterers. In the θ-φ projections there also appear to be a series of vertical lines situated near these arcs and representing repeated bouncing and subsequent sliding off the same scatterer. The lines are most pronounced when elasticity is low, and tend to fade when elasticity increases. Since trajectories accumulate in the regions represented by the sliding and bouncing structures, they map in concentrated groups onto other parts in the Poincaré section, propagating the attractor's fractal structure.

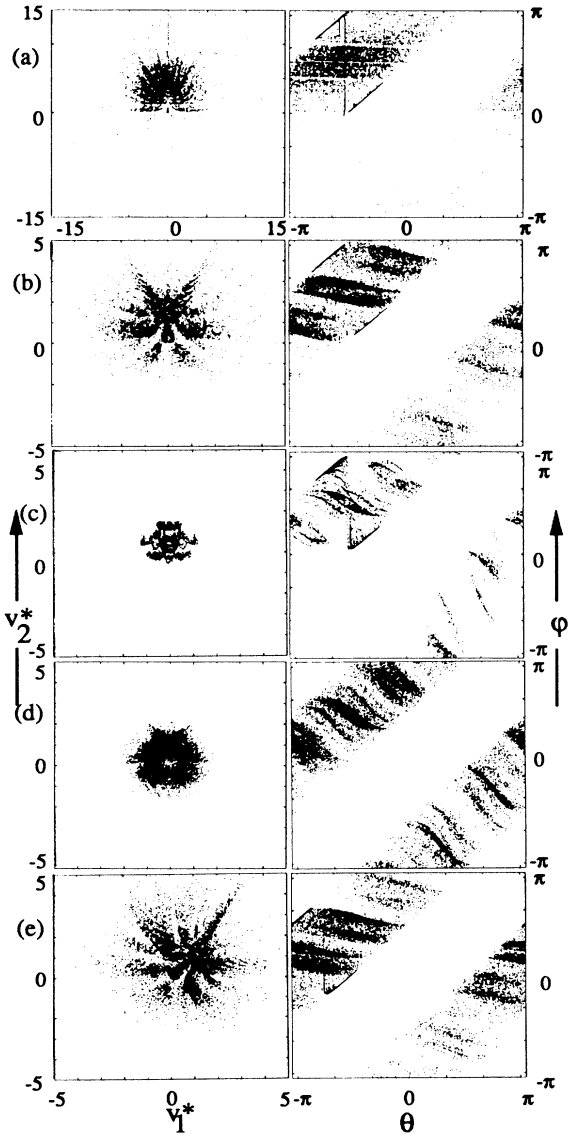

FIG. 14. Examples of strange attractors on the Poincaré map. Velocity space projections and θ-φ projections. (a) Hexagonal lattice: $\beta=90°, \gamma=0.1, e=0.1$. (b) Hexagonal lattice: $\beta=90°, \gamma=0.5, e=0.5$. (c) Hexagonal lattice: $\beta=90°, \gamma=0.85, e=0.5$. (d) Hexagonal lattice: $\beta=90°, \gamma=0.85, e=0.8$. (e) Hexagonal lattice: $\beta=45°, \gamma=0.5, e=0.5$.

Further conclusions can be drawn from the existence of these dense structures. Figure 14(c) shows a low-energy chaotic attractor. Such attractors follow periodic orbits until crises are encountered; the trajectory may then engage in one of two new periodic orbits. The bifurcation seen in Fig. 13 involves a low-energy attractor. Domination of the arcs at $\mathbf{v}=\mathbf{0}$ and its images is clear. These structures represent the bouncing and sliding which all homoclinic orbits must undergo when near the fixed point. Such structures demonstrate the important role played by the fixed point and homoclinic orbits in low-energy chaos. Indeed, one may reassess the importance of homoclinic orbits in the other strange attractors by noting how pronounced the arc at $\mathbf{v}=\mathbf{0}$ is. The less pronounced the arc, the less important the role of homoclinic orbits and the more important the role of convexity in decorrelation (and vice versa).

Figure 14(d) shows a strange attractor at high elasticities. The detailed structure exhibited by other cases is lost here. This observation is consistent with convexity being the mechanism for decorrelation. Nevertheless, it remains clear that the attractor projects itself in lattice-axis directions. The importance of these directions becomes even clearer when Fig. 14(e) is examined. Here, the fingers still project in the lattice direction, even when the direction of gravity is neither along a major axis nor along a significant minor axis.

V. STATISTICAL RESULTS

A. Ergodicity

The attractors on the Poincaré map for one trajectory appear almost identical to the corresponding attractors on the map for several trajectories. This implies ergodicity on the attractor, wherein time averages and phase-space averages are equal. To the extent that this is generally true, each steady-state trajectory is equivalent to the attractor for the entire phase flow. In such circumstances, one can merely select any arbitrary trajectory and find long-time averages. These averages equal en-

semble averages over phase points on the attractor for ergodic systems.

Further numerical evidence points to the ergodicity of Galton-board systems, as summarized in Table I. A close correspondence between ensemble averages and trajectory time averages is observed for a diverse set of cases, including both periodic and chaotic orbits. As a cautionary note, it should be pointed out, however, that some variation exists in the trajectory time averages if different cutoff times are chosen. There also exist variations in ensemble averages for differing ensemble sizes. Nevertheless, strong empirical evidence exists for ergodicity. Ergodicity would support our observations that ensemble averages approach long-time stationary values that are independent of initial conditions. Any deviations from such steady-state behavior appear as noise (disregarding the periodic cases). Moreover, these deviations become smaller with increasing ensemble size. All trajectories sample the attractor without bias, per the requirement of ergodicity. Fluctuations in steady ensemble averages for periodic cases also wane as ensemble size is increased. This is consistent with the existence of ergodicity in the periodic attractor.

B. Terminal velocity and dispersion

Each point in Fig. 15 represents a mean terminal velocity for a given gravity direction, lattice density, and elasticity. We use the term "terminal velocity" to indicate the limiting *average* velocity of an ensemble. Since the lattice geometry examined was square, only gravity directions from 0° to 45° are represented. Data for the remaining directions may be filled in by reflecting this sector about symmetry axes. A mean terminal velocity exists since velocity space constitutes a part of phase space. The attractor would then have a mean velocity value. Moreover, since ergodicity apparently exists, a mean terminal velocity necessarily results since the ensemble average equals the average velocity of the attractor. One obvious conclusion gleaned from Fig. 15 is that mean terminal velocity is substantially dependent upon the orientation of gravity relative to the lattice, particularly with respect to the lattice axes. Moreover, although not shown in the figure, given a particular relative orientation of gravity, all terminal velocities are biased towards the major-axis direction, including chaotic states. Portions of scatterers are shielded by other scatterers in a systematic manner, tending to force particles along major-axis directions. This effect is more pronounced when periodic states are involved; in particular, terminal velocities follow lattice axes regardless of the direction of gravity. The important role played by major and minor axes is once again evident.

TABLE I. Examples of statistical averages for systems exhibiting ergodicity.

Quantity	Ensemble steady state	Trajectory time average
	$\gamma=0.5, e=0.5, \psi=60°, \beta=90°$	
$\langle v_1 \rangle$	0.0	0.0
$\langle v_2 \rangle$	0.66	0.66
σ_v^2	1.5	1.5
	$\gamma=0.5, e=0.5, \psi=60°, \beta=45°$	
$\langle v_1 \rangle$	0.47	0.46
$\langle v_2 \rangle$	0.55	0.57
σ_v^2	1.75	1.78
	$\gamma=0.5, e=0.5, \psi=60°, \beta=1.0$ rad	
$\langle v_1 \rangle$	0.5	0.47
$\langle v_2 \rangle$	0.8	0.78
σ_v^2	3.0	2.70
	$\gamma=0.5, e=0.1, \psi=60°, \beta=90°$	
$\langle v_1 \rangle$	0.0	0.0
$\langle v_2 \rangle$	0.43	0.43
σ_v^2	0.23	0.22
	$\gamma=0.5, e=0.5, \psi=90°, \beta=60°$	
$\langle v_1 \rangle$	0.33	0.33
$\langle v_2 \rangle$	0.63	0.66
σ_v^2	1.80	1.90

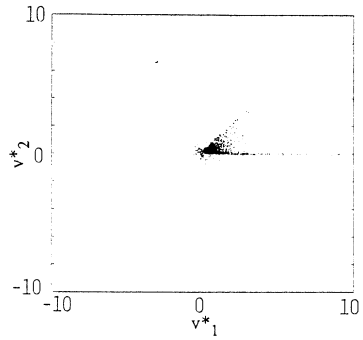

FIG. 15. Mean terminal velocities for a square lattice. Each point represents one set (β,γ,e).

Another interesting result concerning terminal velocity, is the existence of such a velocity for perfectly elastic cases. Figure 16 shows the time evolution of the ensemble velocity for a perfectly elastic case. This velocity appears to either approach an asymptotic value (despite large fluctuations around that value), or it appears to change at a very slow rate (with fluctuations that virtually swamp any detectable trend). The fluctuations are a consequence of finite ensemble size.

Numerical evidence supports the premise that the strange attractors and repellers present in Galton-board systems are ergodic. To the extent this is true, one may treat the systems as a random walk in the positional plane, where the probability of moving between $\mathbf{x}$ and $\mathbf{x}+\Delta\mathbf{x}$ after the Nth collision is dictated by the attractor. Since the attractor possesses a "cut-and-paste" demeanor, little observable correlation exists between one point in Σ and its image under the Poincaré map. Hence the walk may effectively be treated as random. Chandrasekhar [26] proves that as N becomes large, the mean-square displacement grows linearly with time, such temporal behavior representing the Lagrangian definition of a diffusive process. Hence one can expect the ensemble

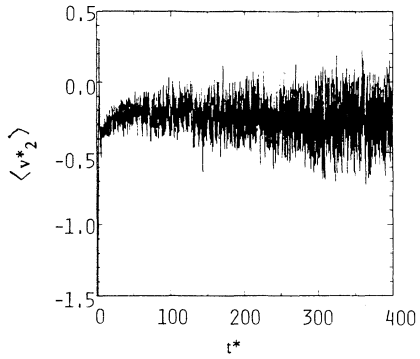

FIG. 16. Terminal velocity for perfectly elastic case. Hexagonal lattice: $\beta=90°, \gamma=0.5$.

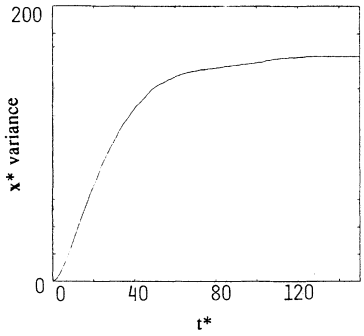

FIG. 18. x variance for periodic case. Hexagonal lattice: $\beta=90°, \gamma=0.5, e=0.1$.

behavior for systems exhibiting strange attractors to be diffusive. Moreover, one can expect the ensemble behavior for systems exhibiting strange repellers to be diffusive also, so long as the ensemble stays near the repeller.

Figure 17 compares the **x**-variance (defined as $\langle \mathbf{x}\cdot\mathbf{x}\rangle - \langle \mathbf{x}\rangle^2$) time evolution for an inelastic case with that for an elastic case. A proper diffusion is observed when $e \neq 1$. When the system is perfectly elastic, the dispersive process fails to be diffusive since the **x** variance possesses a $t^{3/2}$ rather than a t^1 dependence. Energy conservation principles explain this as follows:

$$\frac{d\langle \mathbf{v}\cdot\mathbf{v}\rangle}{dt} = \left\langle \frac{d(\mathbf{v}\cdot\mathbf{v})}{dt} \right\rangle = \left\langle 2\mathbf{v}\cdot\frac{d\mathbf{v}}{dt} \right\rangle = \langle 2\mathbf{v}\cdot\mathbf{g}\rangle = 2\mathbf{g}\cdot\langle \mathbf{v}\rangle \ .$$

However, the existence of a terminal velocity requires that $\langle \mathbf{v}\rangle$ be a constant, whence

$$\langle \mathbf{v}\cdot\mathbf{v}\rangle = 2\mathbf{g}\cdot\langle \mathbf{v}\rangle t + \text{const} \ ,$$

leading to the conclusion that

$$|\mathbf{v}_{\text{relative}}| \sim t^{1/2} \ .$$

For random walks, the **x** variance is proportional to the system's characteristic velocity. This velocity is governed by the ensemble's velocity variance. Since the rate at which each step of the random walk is taken tends to be much faster than the rate of increase of the **v** variance, the latter variance increase may be accounted for as a $t^{1/2}$ scaling. Hence the total **x** variance dependence is expected to be $t^{3/2}$, as observed in the simulations [27].

Figure 18 shows an **x**-variance evolution for a periodic case. The variance approaches a constant that is relatively insensitive to ensemble size. Such behavior constitutes a severe violation of physical expectations for dispersive media. Nevertheless, it is a natural consequence of the periodicity: since each trajectory stabilizes onto a *unique* periodic attractor in the same fashion, each trajectory necessarily moves in the same direction at the same rate, i.e., the **x** variance reaches a steady value. This constitutes yet another statistical manifestation of the complex phase-space structure intrinsic to Galton boards.

Finally, Fig. 19 shows the **x** variance evolution for a periodic case manifesting a symmetric pair of periodic cycles. These cycles constitute two attractors in the same phase space with disjoint basins of attraction [an example of scenario (iv) given in Sec. III B]. One cycle proceeds in the positive x_1 direction, whereas the other proceeds in the negative x_1 direction. Initially, we see the expected chaotic transient (wherein the **x** variance grows linearly with time). However, once the trajectories begin to stabilize into their respective orbits, half move at a constant velocity in one direction while the other half move at a constant velocity in the opposite direction. The **x** variance then grows with the square of time. A bimodal distribution results with the two packets receding from each

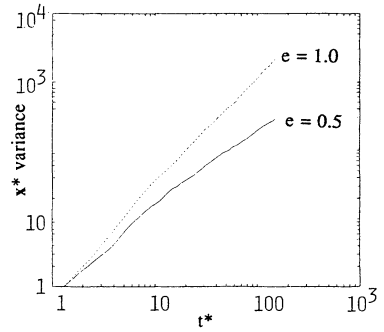

FIG. 17. **x**-variance dependence on elasticity. Hexagonal lattice: $\beta=45°, \gamma=0.5, e=0.5$ and 1.

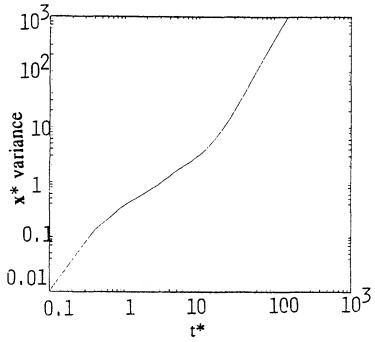

FIG. 19. **x** variance for symmetric periodic case. Hexagonal lattice: $\beta=90°, \gamma=0.8, e=0.46$.

other at constant speed. Moreover, each packet maintains a fixed shape which does not disperse. Hence, even greater complexity results from the subtleties of the phase flow's structure.

VI. CONCLUSIONS

The Galton board's phase flow structure exhibits many subtle characteristics. Lattice axes play a dominant role in stability, phase flow topology, and statistical observations. Smale horseshoes are generated by homoclinic orbits whose existence is dictated by system characteristics. The horseshoes lead directly to deterministic chaos in the system. These horseshoes may be created by increasing system elasticity, decreasing lattice density, or breaking system symmetries. Trajectory instability arises from scatterer convexity and from homoclinic orbits defined by the lattice geometry as well as by the direction of lattice axes relative to gravity. Trajectory stability arises from inelasticity and trajectory path restrictions imposed by lattice density. A subtle balance between instability and stability determines which behavior ultimately results.

Unfortunately, there remains an unsatisfactory lack of mathematical rigor in the given analysis. Few of the suggestions given in Sec. II and III are backed by solid proof or derivation. Therefore, one important line of investigation is the precise derivations of claims made in those sections. But the most serious obstacle to such an investigation is the lack of *a priori* knowledge of period orbit structures and homoclinic cycles. If one can systematically identify where such structures exist without resorting to the numerical computations, one can probably identify certain local characteristics of the bifurcation, based on Melnikov's method or similar techniques [25]. Another avenue for future study is a quantitative analysis of the terminal velocity and diffusivity of cases with chaotic attractors. Another possibility is the classification of stable periodic and quasiperiodic cases via the power spectrum. Here the velocity autocorrelation function will be useful.

Though there are many avenues of investigation yet to pursue, several things can be concluded from our present investigation. The general assertion that Galton boards represent random processes in nature appears unsupported by theory, at least to the extent that our model mirrors the true physics of the phenomena. Although most cases exhibit sensitivity to initial conditions, well-behaved periodic attractors nevertheless occupy a significant fraction of parameter space. These periodic attractors are *not* pathological. Furthermore, the bifurcation structure is not straightforward, and the cases exhibiting strange attractors vary in texture. Finally, qualitative complexity manifested by the diverse phase flow topology is severe, and is observable even at statistical levels. The Galton board reveals intricacies in behavior that belie its superficial simplicity.

ACKNOWLEDGMENTS

The authors wish to thank Professors S. Strogatz and R. A. Brown as well as Dr. D. A. Edwards for useful comments. This material is based upon work supported by the National Science Foundation. A. L. was supported by the National Science Foundation as well as by the Shell Companies Foundation. H.B. was supported by the Office of Basic Energy Sciences of the Department of Energy.

*Electronic address: ithron@athena.mit.edu

[1] M. Kac, Sci. Am. **211**, 92 (1964).
[2] H. Brenner and D. A. Edwards, *Macrotransport Processes* (Butterworth-Heinemann, Stoneham, MA, 1993); J. S. Chung, K. H. Lee, and D. Stroud, Phys. Rev. B **40**, 6570 (1989).
[3] B. Moran, W. G. Hoover, and S. Bestiale, J. Stat. Phys. **48**, 709 (1987).
[4] W. G. Hoover *et al.*, Phys. Lett. A **133**, 114 (1988).
[5] Ya. G. Sinai, Russ. Math. Surv. **25**, 137 (1970).
[6] I. Kubo, Nagoya Math. J. **61**, 1 (1976).
[7] L. A. Bunimovich and Ya. G. Sinai, Commun. Math. Phys. **78**, 247 (1980).
[8] L. A. Bunimovich and Ya. G. Sinai, Commun. Math. Phys. **78**, 479 (1980).
[9] J. Machta and R. Zwanzig, Phys. Rev. Lett. **50**, 1959 (1983).
[10] B. Bagchi, R. Zwanzig, and M. C. Marchetti, Phys. Rev. A **31**, 892 (1985).
[11] J.-P. Bouchaud and P. Le Doussal, J. Stat. Phys. **41**, 225 (1985).
[12] J. Machta and B. Reinhold, J. Stat. Phys. **42**, 949 (1986).
[13] A. Zacherl *et al.*, Phys. Lett. **114A**, 317 (1986).
[14] B. Friedman and R. F. Martin, Jr., Physica D **30**, 219 (1988).
[15] S. P. Das and M. H. Ernst, Physica A **153**, 67 (1988).
[16] J. Guckenheimer and P. Holmes, *Nonlinear Oscillations, Dynamical Systems, and Bifurcations of Vector Fields* (Springer, New York, 1983).
[17] H. E. Lehtihet and B. N. Miller, Physica D **21**, 93 (1986).
[18] M. Henon, Physica D **33**, 132 (1988).
[19] B. N. Miller and K. Ravishankar, J. Stat. Phys. **53**, 1299 (1988).
[20] M. Franaszek and H. M. Isomaki, Phys. Rev. A **43**, 4231 (1991).
[21] Z. J. Kowalik, M. Franaszek, and P. Pieranski, Phys. Rev. A **37**, 4016 (1988).
[22] An exceptional case occurs when $\Delta \mathbf{v} = \text{const} \times \mathbf{g}$. The difference in velocities then represents a displacement along the trajectory path, which does not constitute a legitimate divergence. The divergence necessary, e.g., for a strange attractor to result, must be transverse to the trajectory path.
[23] Recall at higher energies, gravitation becomes irrelevant according to the prescription given in Sec. II D, i.e., one achieves the DLG limit. Then for trajectories to scatter "left" or "right" relative to the incident trajectory will depend only on that trajectory's angle of incidence. Left-scattered trajectories become quickly decorrelated from right-scattered trajectories. But the manifold in phase

space that separates left scattering and scattering is merely a continuation of the hyperbolic manifold. But recall that the phase behavior of dissipative Lorentz gases is independent of v. Therefore, the hyperbolic manifold will extend into indefinitely large-v regions, where "large" is defined as per Sec. II D.

[24] For a curve to be tangent to N scatterers requires $2N$ free parameters (positional and velocity constraints). Since a parabola has only three free parameters, no boundary maps onto another on more than a finite number of points.

[25] S. Wiggins, *Global Bifurcations and Chaos: Analytical Methods* (Springer, New York, 1988).

[26] S. Chandrasekhar, in *Selected Papers on Noise and Stochastic Processes,* edited by N. Wax (Dover, New York, 1954), pp. 3–91.

[27] J. Piasecki and E. Wajnryb, J. Stat. Phys. **21**, 549 (1979). We mention an important result from this paper: A dilute, elastic, aperiodic Lorentz gas exhibits no terminal velocity and its relative velocity scales as $t^{1/3}$. Comparing this result to ours suggests that the order induced by a lattice structure changes the statistical behavior of a scattering medium. More investigation in the purely elastic regime is necessary to make a more serious evaluation of the effect of lattice order on macroscopic observables.